ILASS 2008
Sep. 8-10, 2008, Como Lake, Italy

Paper ID ILASS08-9-2

COMPLEMENTARY EXPERIMENTAL AND COMPUTATIONAL STUDY OF A DROP IMPACTING A SHALLOW POOL

Nils P. van Hinsberg*, Edin Berberović°, Ilia V. Roisman*, Suad Jakirlić*, Cam Tropea*

*Chair of Fluid Mechanics and Aerodynamics, Technische Universität Darmstadt, Darmstadt, Germany
°Chair of Energy Technology and Process Engineering, University of Zenica, Bosnia and Herzegovina

ABSTRACT
In this paper experimental and numerical investigations of a normal drop impact onto a liquid film of a finite thickness are performed. The liquids used in the experiments and calculations are distilled water and isopropanol and the impact occurs in ambient air. The shape of the crater formed upon the impact is observed using the high-speed video system. In numerical calculations, unsteady Navier-Stokes equations for incompressible flow are solved using the finite volume method. The effects of different drop impact velocities, liquid film thicknesses and physical properties of the liquids, including surface tension, on the time evolution of the crater formed within the film upon the impact are investigated. Using the experimental and numerical results, the dynamics of drop impact on liquid surfaces is analyzed, focusing on the depth and diameter of the crater.

INTRODUCTION

Splashing of drops on liquid layers is encountered frequently in nature and leads to different phenomena like air bubble formation during heavy rain, formation of a crown like liquid sheet with detaching secondary droplets, and ejection of a liquid jet from the region of impact. Investigations of drop impact onto liquid films have also importance in various engineering fields. It is important in soil erosion, in agriculture for the dispersion of seed and microorganisms and in many other technical applications such as spray coating and cooling, paint-spraying and internal combustion engines with direct fuel injection, where the fuel is sprayed into engine cylinders in the form of small droplets which splash on the inner walls of cylinders. It is of importance also in atmospheric sciences for separation of electrical charges by the liquid disintegration during splashing [1]. Also rainwater separation in water boxes in air-conditioning systems in automobiles requires knowledge and control over this process [2].

For many applications of practical interest, the hydrodynamics, as well as physical and chemical mechanisms governing the process of liquid displacing a fluid from a solid surface are still unresolved. The main reason is the difference between the molecular or, at best, submicroscopic length scales at which the process in reality takes place and the macroscopic scales accessible by experimental equipment, which are of the order of, at best, tens of micrometers. In this study, experimental and numerical investigations of a normal drop impact onto a liquid film of a finite thickness are performed. The formation and evolution of the crater formed upon the impact beneath the surface are investigated at various film thicknesses, drop impact velocities and using two different liquids.

EXPERIMENTAL METHOD

Experimental measurements were performed using the experimental setup shown in Fig.1 [3]. Drops are generated using a syringe pump with constant preset flow rate. The drop is formed at the tip of the needle and grows until its weight exceeds the surface tension force. After the drop detaches from the needle it falls and passes a light barrier before reaching the center of a cylindrical vessel of 90 mm diameter made of Plexiglas. The cylinder is large enough to avoid effects of wave reflections from the sides with the impact process. The light barrier activates an electronic delay circuit that triggers the imaging system, consisting of two CCD cameras, one backlit by a stroboscope and the other by a PIV laser. In order to investigate the influence of liquid properties on the crater evolution, two liquids were used in experiments, distilled water and isopropanol. The fluid of the drop and the film is the same in all experiments.

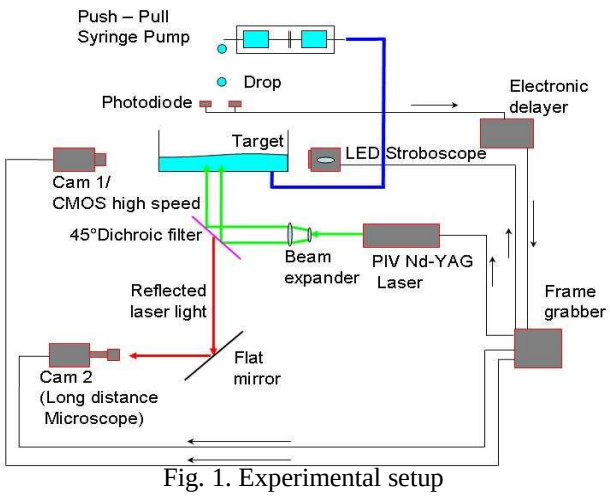

Fig. 1. Experimental setup

Comparison of different cases is enabled by the use of the corresponding non-dimensional numbers governing the impact process: Weber number $We=\rho U^2 D/\sigma$ giving the relation of inertial to surface tension forces, Ohnesorge number $Oh=\mu/(\sigma\rho D)^{1/2}$ giving the relation of viscous to surface tension forces, dimensionless film thickness $H=h/D$ and dimensionless time $T=tU/D$. In the above expressions μ, σ, and ρ are dynamic viscosity, surface tension coefficient and density of the liquids used, D and U are the diameter and the impact velocity of the drop, and h is the film thickness. The initial drop diameter is 2.97 mm for distilled water and 2.12 mm for isopropanol. The drop impact velocity (velocity just before the drop reaches the film surface) is calculated from a distance measurement and a preset time delay between subsequent exposures. Thus, for distilled water the impact velocity varied from 1.68 m/s and 2.91 m/s and for isoropanol from 1.7 m/s to 2.83 m/s. The liquid film thickness was varied from 1.5 mm to 6 mm for distilled water and from 1.06 mm to 4.24 mm for isopropanol, yielding the non-dimensional film thickness of 0.5 to 2 for both liquids. The film thickness is held constant with an error in thickness of 3% to 7% for distilled water and 2% to 10% for isopropanol. The physical properties of liquids and ranges of the non-dimensional numbers are given in Tab. 1.

Tab. 1. Physical properties of liquids used and ranges of non-dimensional numbers

	Distilled water	isopropanol
Density ρ, kg/m^3	999	805
Dynamic viscosity μ, Pas	$9.9\cdot10^{-4}$	$2.3\cdot10^{-3}$
Surface tension coefficient σ, N/m	$7.27\cdot10^{-2}$	$2.36\cdot10^{-2}$
Ohnesorge number Oh, -	0.0021	0.0112
Weber number We, -	137 – 312	204 – 644

COMPUTATIONAL METHOD

In addition to experiments, numerical simulations of the cases studied were performed. The process of drop impact is generally difficult to simulate because of several reasons. It is a highly transient flow process, with characteristic time scales ranging down to a few microseconds. The length scales can also be very small, sometimes of the order less than one micrometer. The known physics of this phenomenon states that there are several competitive effects influencing the flow field during, and the final outcome after the impact: gravity, viscous, inertial and surface tension forces. In particular the effects of surface tension or capillarity, which drives the process after the inertial forces become small, are hard to capture due to discontinuity of physical properties at the interface. In a classical VOF method, a transport equation for an indicator function, usually the volume fraction of one phase, is solved in addition to equations of motion. Here another approach is used, the equation for volume fraction is derived based on a two-fluid formulation, similar to the model in [4]. The mathematical model is described by the following equations for conservation of mass, volume fraction and linear momentum:

$$\nabla\cdot\mathbf{U}=0 \tag{1}$$

$$\frac{\partial\gamma}{\partial t}+\nabla\cdot(\mathbf{U}\gamma)+\nabla\cdot\left[\mathbf{U}_r\gamma(1-\gamma)\right]=0 \tag{2}$$

$$\frac{\partial(\rho\mathbf{U})}{\partial t}+\nabla\cdot(\rho\mathbf{U}\mathbf{U})=-\nabla p_d-g\cdot\mathbf{x}\nabla\rho+\nabla\cdot\mathbf{T}+\mathbf{f}_\sigma, \tag{3}$$

where $\mathbf{U}$ is velocity vector, γ is volume fraction of liquid phase, $\mathbf{U}_r$ is a vector of relative velocity, or the so-called compression velocity, ρ is density, p_d is modified pressure obtained by removing the hydrostatic contribution from the physical pressure, $\mathbf{x}$ is position vector, $\mathbf{T}$ is viscous stress tensor and $\mathbf{f}_\sigma$ is force due to surface tension. The equation for volume fraction, Eq. (2), contains an additional convective term, which provides the necessary compression of the interface, rather than using a compressive differencing scheme for convection. This term is active only at the interface and does not affect the solution outside this region. In addition to properly reflecting the physics of the flow, the main advantage of such formulation is the possibility of capturing the interface region much more sharply compared to the classical VOF approach. Numerical diffusion, unavoidably introduced through the discretization practice, can be controlled through the compression term, thus allowing sharp interface capturing.

For the discretization of the third term in the Eq. (2) the compression velocity is formulated based on the maximum velocity magnitude at the interface region. Two immiscible fluids are considered as one effective fluid throughout the domain, the physical properties of which are calculated as weighted averages based on the distribution of the liquid volume fraction, thus being equal to the properties of each fluid in their corresponding occupied regions and varying only across the interface:

$$\rho=\gamma\rho_l+(1-\gamma)\rho_g \text{ and} \tag{4}$$

$$\mu=\gamma\mu_l+(1-\gamma)\mu_g, \tag{5}$$

where ρ_l and ρ_g are densities of liquid and gas, respectively. Both fluids are considered to be Newtonian and incompressible, and the viscous stress tensor is linearly related to the rate of strain tensor according to Stokes' law. Body forces due to pressure gradient and gravity are implicitly accounted for by the first two terms on the r.h.s. of the Eq. (3). The surface tension force is evaluated based on the Continuum Surface Force (CSF) model [5]:

$$\mathbf{f}_\sigma=\sigma\left[-\nabla\cdot\left(\frac{\nabla\gamma}{|\nabla\gamma|}\right)\right]\nabla\gamma, \tag{6}$$

The computations were performed by the open source CFD Toolbox OpenFOAM (www.open.co.uk/openfoam) using cell-center-based finite volume method on a fixed unstructured grid. Coupling between pressure and velocity is ensured by PISO algorithm for unsteady flows. For the discretization of the convective terms in Eq. (2) it is important to assure boundedness of the solution. Here, blending between upwind and central differencing was used, with a nonlinear varying blending factor, which is evaluated based on the ratio between flux gradients calculated at adjacent cell faces and cell

centers. Discretization of unsteady terms is accomplished by Euler implicit scheme. The calculations are performed using a self-adapting time step size which is adjusted during the calculation at the beginning of every time iteration loop in order to ensure stability of the solution procedure. The new time step size is calculated based on predefined maximum Courant number equal to 0.2 and the time steps were on the order of 10^{-7} s to 10^{-5} s.

The numerical grid used in computations is an axisymetric slice in 2D with dimensions of 45 mm × 45 mm in the vertical plane and one cell in azimuthal direction, shown in Fig. 2.

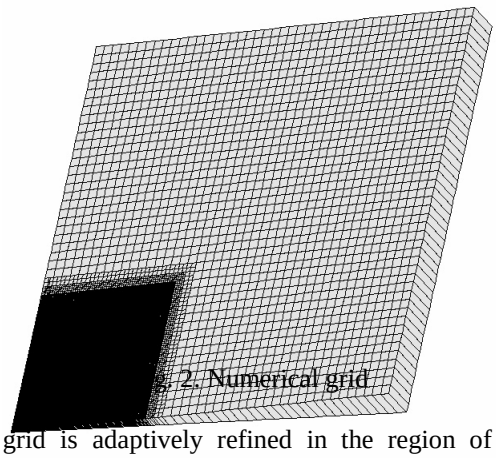

Fig. 2. Numerical grid

The grid is adaptively refined in the region of interest where the crater is formed. In previous calculations on coarser grids it could be observed that the initialized velocity and pressure fields are not significantly affected at a radial distance greater than approximately one third of the radial direction, since the process of drop impact occurs very fast. Therefore grid refinement was applied only in this region of the solution domain, the finest grid having in total about 150 000 cells.

The boundary conditions correspond to the geometry of the experiments. In addition to the axis of symmetry, the no-slip condition is prescribed at the bottom and to the right side boundary, and the top boundary was open with prescribed total pressure consisting of static and dynamic pressure and allowing the pressure to be adjusted according to the calculated velocity field. Since a clear contact of the crater with the bottom of the cylinder could not be observed in the experiments, it could not be identified if the surface around the central axis becomes totally free of liquid. Therefore, wall adhesion was not taken into account, i.e. a static contact angle of 90° was applied at the walls, corresponding to zero-gradient condition for the volume fraction equation.

At the initial time, the distribution of volume fraction is prescribed throughout the domain, defining the position and the shape of the interface at the beginning of the calculation. Initialization of pressure is done by setting hydrostatic pressure distribution within the film and capillary pressure in the drop corresponding to its diameter. The drop is placed at an initial distance from the film surface corresponding to time interval of 250 μs, which is considered to be sufficient for the flow development before the impact. Since the distance is very small, the effects of gravity are negligible and the initial drop velocity is set equal to the drop impact velocity from experiments.

RESULTS

Comparison between exposures from experiments and results of simulations at different times for $H = 2$ is given in Fig.3 for 1-propanol and Fig.4 for distilled water.

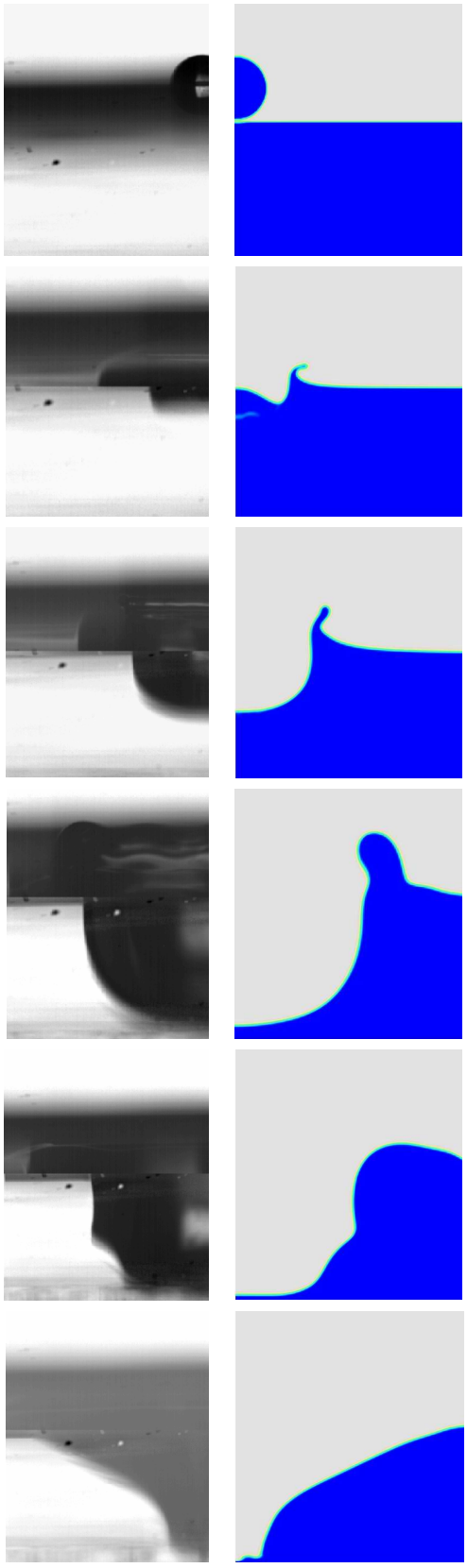

Fig. 3. Crater shape, experiment (left) and simulations (right). We = 392, tU/D_{drop} = 0, 1.08, 2.71, 10.84, 21.68, 31.44 (from top to bottom);

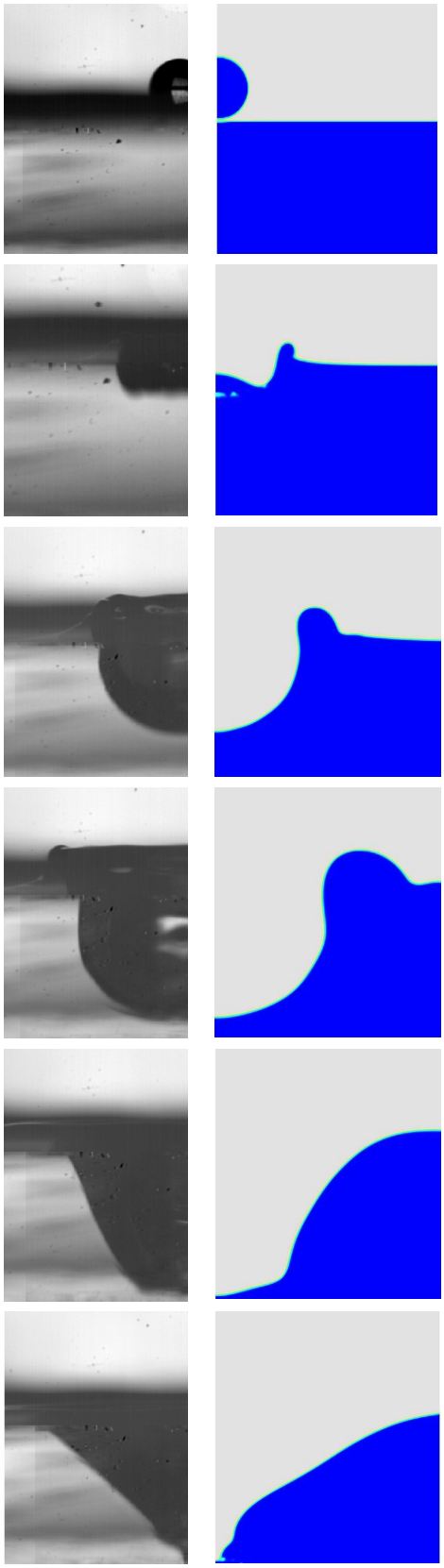

Fig. 4. Crater shape, experiment (left) and simulations (right). We = 215, tU/D_{drop} = 0, 1.21, 4.03, 8.06, 16.13, 20.97, (from top to bottom)

Immediately upon impact, a small circumferential free liquid film (the corona) is ejected upward. The geometry of this free film (its height, shape and thickness) depends on the drop impact velocity, liquid used and liquid film thickness. Inside the liquid film the drop impact leads to the formation of a cavity (crater), which penetrates into the film and simultaneously expands radially. During the spreading period inertial forces are dominant over viscous and capillary forces since the Weber number is much higher than unity. After reaching the maximum diameter, the crater begins a receding motion, driven by capillary forces, and collapses around the central axis. It can be seen that crater shape changes from spherical in the advancing motion to conical during the receding motion. A capillary wave is observed at the surface of the crater in Fig.3 which is created inside the circumferential upward directed film and travels downwards along the crater surface. This behavior is clearly resolved in the simulations. The capillary wave is observed here only when isopropanol is used, whereas it could not clearly be seen in impacts of distilled water (Fig.4), as a consequence of higher surface tension of distilled water. In the results of simulations it can also be seen that during the first stages of impact the cavity has a concave surface in its upper part, and the crater is fully formed afterwards until its bottom becomes convex. This could not be observed in experiments and consequently, for comparison purposes, the measured crater depth is related to the lowest point at the edge of the crater seen in the results of simulations.

For a quantitative analysis, crater depth and diameter are made dimensionless through division by drop diameter, and the measured values are compared to predicted ones. In the experiments the depth is measured at the lowest point of the crater observed in photographs, and the diameter is determined at a half film thickness, i.e. for z/h=0.5, where z is the vertical distance measured from the free surface of the film. In simulations, depth and diameter are determined using computational cells where volume fraction has a value $\gamma \geq 0.5$.

Plots of dimensionless crater depth and diameter against dimensionless time for isopropanol are given in Fig.5 and Fig.6, and for distilled water in Fig.7 and Fig.8, respectively. It can be seen that the crater penetrates into the liquid film with a constant velocity until it reaches and nearly touches the bottom. It then resides a certain time period near the bottom before it starts to retract. The dimensionless time at which the crater reaches the bottom is approximately equal for both fluids. However, the retraction motion begins sooner when distilled water is used (Fig.5 and Fig.7). Also the diameter of the crater reaches its maximum value at lower time for distilled water compared to isopropanol (Fig.6 and Fig.8). One can conclude that for liquids with lower surface tension (isopropanol in this study) the crater propagates downward equally fast as for liquids with higher surface tension, but the spreading of the crater is much more pronounced, providing a larger maximum diameter.

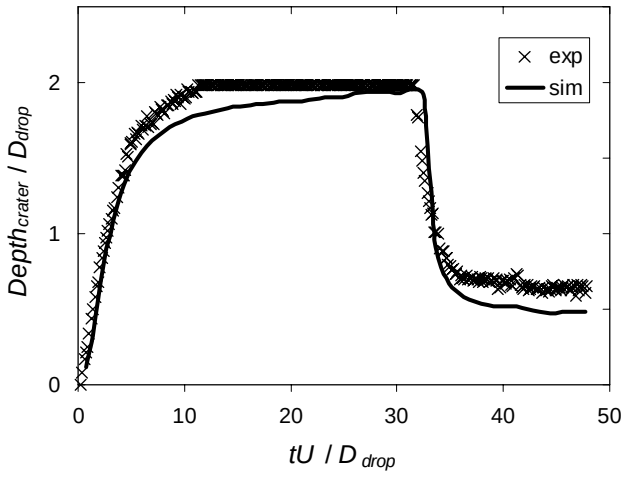

Fig. 5. Crater depth, We = 392

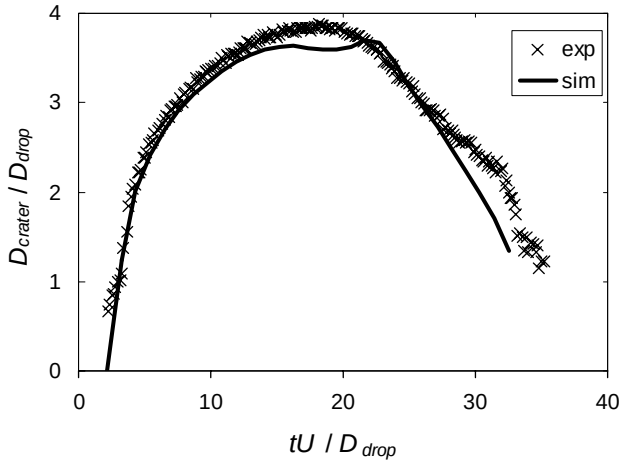

Fig. 6. Crater diameter, We=392

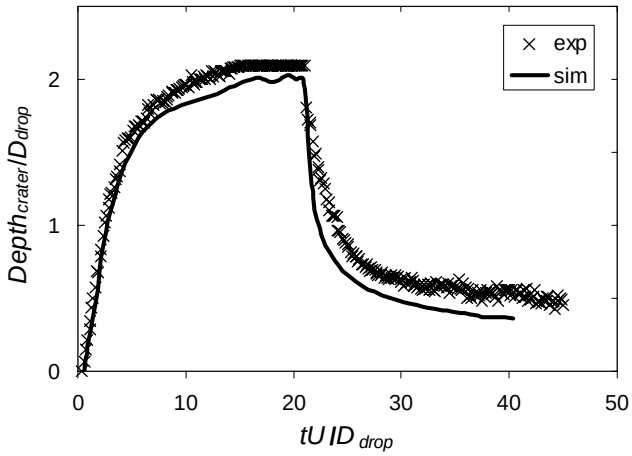

Fig. 7. Crater depth, We=215

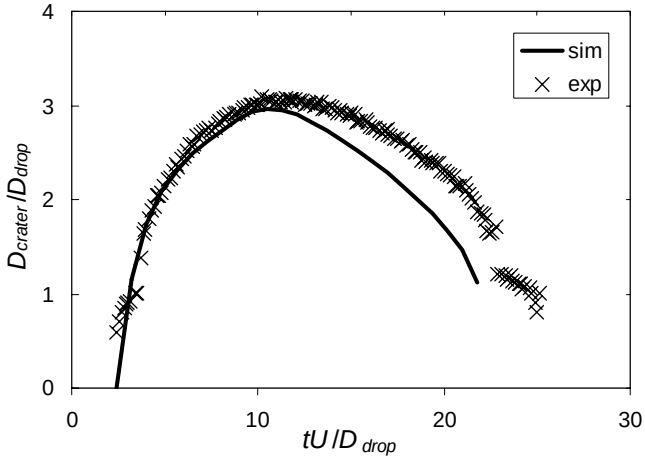

Fig. 8. Crater diameter, We=215

In fact, for higher surface tension, inertia is overcome earlier by capillary forces, leading to a lower maximum crater diameter and an earlier retraction. The capillary wave from Fig.3 is represented in Fig.6 as a sudden increase in crater diameter at a time when the wave passes a half-film thickness. Experimental results are very well predicted in the simulations, with a small disagreement for crater diameter at We = 215. Pressure and velocity fields for impact at We = 392 and $H = 2$ are given in Fig.9 at the time the drop first touches the film and in Fig.10 at a later time instant.

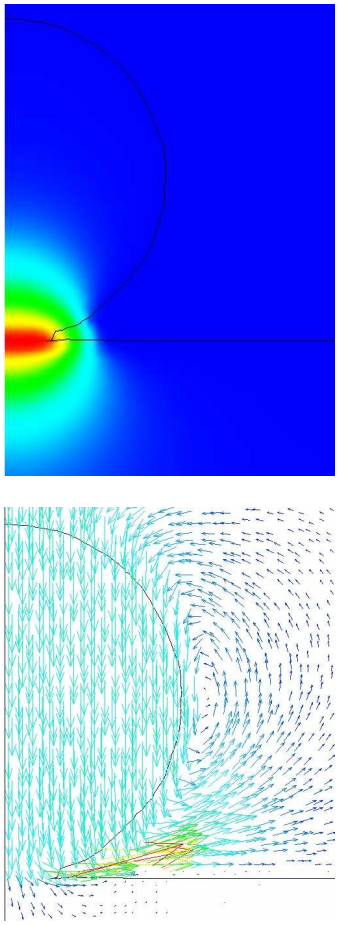

Fig. 9. Pressure field (top) and velocity fields (bottom), We=392, $tU/D_{drop} = 0$

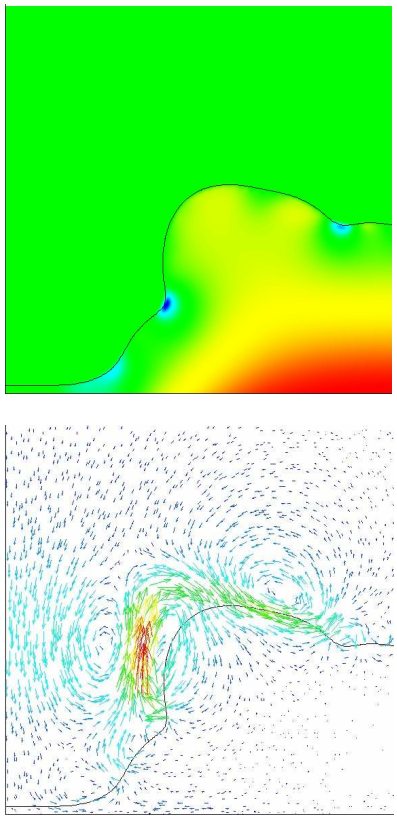

Fig. 10. Pressure field (top) and velocity fields (bottom), We=392, $tU/D_{drop} = 21.68$

For clarity, the velocity field is shown using random mask points. It can be seen in Fig.9 that, at the moment when the drop touches the liquid film, a high pressure is formed in the region of contact. The highest pressure is not in the central axes, but at the edge of the circumferential area of contact. As a consequence of this, high velocities are obtained leading to ejection of fluid in a radially upward direction. In Fig.10 it can be seen that there exists a region beneath the crater surface where negative pressure occurs. This can be used to explain the creation and movement of the capillary wave. For the fluid with lower surface tension, the negative pressure is strong enough to overcome capillary forces and a small amount of liquid at the surface is pulled into the film, which creates the surface wave. The wave travels downwards driven by the vertical components of the velocity field. For the fluid with higher surface tension, the negative pressure being built is weaker, and as a consequence, a clear capillary wave is not observed in either experiments or in simulations.

CONCLUSION

In this paper the dynamics of the crater formed upon the impact of a single drop onto a liquid film was investigated using experimental measurements and numerical simulations. The dynamics of drop impact on liquid surfaces is analyzed, focusing on the evolution of the crater formed beneath the surface upon the impact. Very good agreement between experiments and simulations is obtained. It was shown that the numerical simulations provide a good tool to investigate and help understanding the complex phenomena arising during a drop impact.

ACKNOWLEDGMENT

The authors would like to thank DAAD (Deutscher Akademischer Austauschdienst) for supporting Edin Berberović through a research scholarship.

NOMENCLATURE

Latin symbols

D	Drop diameter	m
$\mathbf{f}$	Body force	N/m^3
h	Film thickness	m
H	Dimensionless film thickness	-
Oh	Ohnesorge number	-
p	Pressure	Pa
t	Time	s
T	Dimensionless time	-
$\mathbf{U}$	Velocity vector	m/s
We	Weber number	-
$\mathbf{x}$	Position vector	m
z	Vertical distance	m

Greek symbols

γ	Volume fraction	-
μ	Dynamic viscosity	Pa s
ρ	Density	kg/m^3
σ	Surface tension coefficient	N/m

Subscripts and superscripts

b	Body force
d	Modified
g	Gaseous phase
l	Liquid phase
r	Relative
γ	Compression coefficient
σ	Surface tension force

REFERENCES

[1] Z. Levin, Charge Separation by Splashing of Naturally Falling Raindrops, *Journal of the Atmospheric Sciences*, vol. 28, pp 543-548, 1971.

[2] J. Urban, B. Weigand, N. Roth, M. Eyselein, K. Trackl, R. Tatschl and A. Raulot, Modeling of Droplet Wall Interaction, *Proc. 6th International Conference on Multiphase Flow*, 2007.

[3] N. P. van Hinsberg, I. V. Roisman and C. Tropea, An Experimental Study of the Crater Evolution by Impact of a drop onto a Shallow Pool, *Proc. 21th Annual Conference on Liquid Atomization and Spray Systems*, 2007.

[4] H. Rusche, Computational Fluid Dynamics of Dispersed Two-Phase Flows at High Phase Fractions, Ph.D. thesis, Imperial College of Science, Technology and Medicine, London, 2002.

[5] J. U. Brackbill, D. B. Kothe and C. Zemach, A Continuum Method for Modeling Surface Tension, *Journal of Computational Physics*, vol.2 pp. 335-354, 1992.

[6] OpenFOAM - The Open Source CFD Toolbox: www.opencfd.co.uk/openfoam/